Recruitment of plasma cells to the bone marrow in primary and secondary immune reactions

Marta Ferreira-Gomes
German Rheumatism Research Centre https://orcid.org/0000-0002-7171-7952
Pawel Durek
German Rheumatism Research Centre
Yidan Chen
Charité-Universitätsmedizin Berlin
Hector Rincon-Arevalo
Charité-Universitätsmedizin Berlin https://orcid.org/0000-0001-5614-7894
Frederik Heinrich
German Rheumatism Research Centre (DRFZ) Berlin https://orcid.org/0000-0001-6097-5422
Franziska Szelinski
Charité-Universitätsmedizin Berlin https://orcid.org/0000-0001-7850-5971
Gabriela Guerra
Deutsches Rheuma-Forschungszentrum Berlin
Ana-Luisa Stefanski
Charité-Universitätsmedizin Berlin https://orcid.org/0000-0001-7689-6454
Antonia Niedobitek
Deutsches Rheuma-Forschungszentrum Berlin
Annika Wiedemann
Charité-Universitätsmedizin Berlin
Marina Bondareva
Deutsches Rheuma-Forschungszentrum Berlin
Jacob Ritter
Charité-Universitätsmedizin Berlin
Katrin Lehmann
German Rheumatism Research Centre
Sebastian Hardt
Charité-Universitätsmedizin Berlin
Christian Hipfl
Charité-Universitätsmedizin Berlin
Sascha Hein
Paul-Ehrlich-Institut
Eberhard Hildt

Paul-Ehrlich-Institut

Mareen Matz

Berlin Institute of Health at Charité-Universitätsmedizin Berlin

Henrik Mei

DRFZ Berlin https://orcid.org/0000-0003-0697-7755

Qingyu Cheng

Charité - Universitätsmedizin Berlin

Van Duc Dang

Deutsches Rheuma-Forschungszentrum Berlin

Mario Witkowski

Charité - Universitätsmedizin Berlin https://orcid.org/0000-0002-8791-5558

Andreia Lino

Deutsches Rheuma-Forschungszentrum Berlin

Andrey Kruglov

German Rheumatism Research Centre

Fritz Melchers

Deutsches Rheuma-Forschungszentrum Berlin

Carsten Perka

Charité-Universitätsmedizin Berlin

Eva Schrezenmeier

Charité-Universitätsmedizin Berlin

Andreas Radbruch

Deutsches Rheuma-Forschungszentrum Berlin (DRFZ), a Leibniz Institute https://orcid.org/0000-0001-5753-0000

Thomas Dörner

DRFZ

Mir-Farzin Mashreghi (mashreghi@drfz.de)

Deutsches Rheuma-Forschungszentrum Berlin https://orcid.org/0000-0002-8015-6907

Article

Keywords:

Posted Date: February 15th, 2023

DOI: https://doi.org/10.21203/rs.3.rs-2378630/v1

Abstract

Bone marrow plasma cells (BMPC) emerge as a consequence of immune reactions and are considered the source of antibodies that protect against recurrent infectious diseases throughout life. Despite their importance, it remains unclear if these cells reflect different activation environments or the differentiation/maturation stages of their precursors. Here we track the recruitment of plasma cells, generated in primary and secondary immune reactions to SARS-CoV-2 spike protein vaccines, to the human bone marrow. Trajectories based on single cell transcriptomes and antigen-receptor clonotypes of antibody-secreting cells exiting the immune reaction and of those residing in the bone marrow, allow to follow the evolution of the immune response to these vaccines, leading to sequential colonization of these cells to different compartments (clans) of BMPC, and their establishment as long-lived (memory) plasma cells. In primary immune reactions, both $CD19^{low}$ (clans 1 and 4) and $CD19^{high}$ (clan 0) BMPC are generated. In secondary immune reactions, mostly $CD19^{high}$ BMPC of the largest compartment (clan 0) are generated, resulting from the reactivation of memory B lymphocytes. The latter is also observed in vaccinated convalescent individuals and upon recall vaccination against diphtheria/tetanus/pertussis (DTP). Thus, humoral immunological memory, i.e. serum antibodies secreted by long-lived memory BMPC, is generated already in the primary immune response, more so in the secondary, and it represents the evolution of the immune response.

Introduction

Long-lived plasma cells are rare cells that reside and rest in dedicated survival niches of the bone marrow (BM), continuously secreting antibodies against previously encountered pathogens[1]. These cells are considered to originate mostly from T cell-dependent B cell activation in secondary lymphoid organs. The concept of long-term humoral immunity through long-lived (memory) plasma cells[2,3] has gained acceptance and attention during the COVID-19 pandemic, as the presence of spike-specific memory plasma cells is a correlate of long-lasting protection against severe disease and death[4,5]. This protection, conferred by stable systemic antibody titers, can last over decades, if not a life time[6]. Despite their relevance, the recruitment of plasma cells from the secondary lymphoid organs into the bone marrow and their establishment there as long-lived plasma cells (BMPC) is not well understood. Plasmablasts of primary and secondary immune reactions might differ in their competence to enter the bone marrow and survive there as long-lived plasma cells[1]. BMPC are heterogeneous with respect to expression of e.g. CD19[7,8], CD38[7], PD-1[8], CD39 and CD326[9], but whether that reflects different environments in their generation or different qualities as BMPC, has remained unclear. It also is unclear whether BMPC are constantly recruited during an immune reaction to the BM or only at the end, when affinity maturation is finished[10–12].

Here, we address these open questions by a global analysis of the transcriptional heterogeneity and antigen receptor repertoire of human BMPC, and follow the recruitment of plasma cells (PC) to the bone marrow in primary and secondary immune reactions to SARS-CoV-2 vaccines. We find 10 clans of BMPC,

differing in and reflecting the instructive signals they received as activated B cells. By comparing the transcriptome signatures of newly generated circulating antibody-secreting cells (ASC) to the transcriptomes of established BMPC, we track the recruitment of PC to the bone marrow in the primary and secondary immune reactions. While PC generated in primary immune reactions to the vaccines are recruited to distinct $CD19^{low}$ and $CD19^{high}$ clans, PC generated in secondary immune responses are nearly exclusively recruited to clan 0 ($CD19^{high}$). While most ASC exiting the immune reaction on day 7 express IgG1, an isotype targeted by IL-21[13,14], ASC exiting later, on day 14 and after 6 or 7 months, also express IgA1 and IgA2, isotypes targeted by TGF-β[15]. ASC expressing IgG2, reflecting instruction by interferons[16], are not as frequently induced by the vaccines. PC recruited to BM in secondary immune reactions are derived from (re)activated memory B cells, while the $CD19^{low}$ BMPC probably reflect the direct output of primary germinal centre reactions. Upon repeated vaccination, spike-specific BMPC are present in most clans, reflecting the evolution of the immune response, the continued recruitment of PC to the BM during an immune reaction, and their long term maintenance there.

Results

Transcriptional and phenotypic heterogeneity of BMPC

Single cell transcriptomes were obtained from 38235 BMPC of eight patients who underwent joint-replacement surgery of the hip (Supplementary Table 1). BMPC were enriched as viable $CD38^{high}CD138^{high}CD3^{-}CD10^{-}CD14^{-}$ or $CD38^{high}CD27^{high}CD3^{-}CD14^{-}$ cells (Supplementary Fig. 1a), stained in addition with DNA-barcoded antibodies for Cellular Indexing of Transcriptomes and Epitopes by Sequencing (CITE-seq), and subjected to single cell transcriptome as well as full length B cell receptor (BCR) sequencing. Cells were clustered according to their transcriptomes and visualized by Uniform Manifold Approximation and Projection for Dimension Reduction (UMAP)[17]. From the 15 defined subpopulations, clusters 2, 3 and 10 were excluded since they contained low quality cells expressing 16.4% (median, MAD = 6.6%) mitochondrial genes and/or a significantly low number of detected transcripts (a median of 453, 842 and 662, respectively; MAD = 133, 266, 152) (Supplementary Fig. 1b). Clusters 7 and 14 represented CD20-expressing B cells and pre-B cells, respectively, and thus were not considered further as BMPC. The remaining 10 clusters (Fig. 1a), present in all 8 patients (Fig. 1b), were classified as BMPC according to their expression of the signature genes *PRDM1*, *IRF4*, *XBP1*, and *SDC1* (Fig. 1c), and of surface proteins, including CD27, CD38 and CD138 (Supplementary Fig. 1c, d). 38% of the BMPC analysed are residing within cluster 0, containing 34% $CD19^{high}$ cells, and predominantly expressing IgA1 and IgG1 antibodies (Fig. 1b-f). Clusters 1 and 4 contain predominantly $CD19^{low}$ cells, 93% and 84%, respectively (Fig. 1c, d). Both clusters 0 and 1 are enriched for IgG1-expressing BMPC (Fig. 1e, f). Cells of cluster 5 represent a population of $XBP1^{low}$ $IRF4^{high}$ IgA1 BMPC, 27% of which do express CD19. They could be derived from systemic TGF-β driven immune reactions. Cluster 4 is enriched for IgA2 and IgM BMPC expressing *IgJ*, *CCR10 and ITGB7*, indicative of a mucosal origin[18] (Fig. 1c-f). Cluster 6 consists of BMPC expressing *CD9* and IgG2, hallmarks of a type II interferon (IFN)-driven

immune reaction (Fig. 1d, e). With cells expressing elevated levels of *STAT1 and IFITM1* (Fig. 1d), cluster 8 represents BMPC generated in a type I IFN response, also supported by gene set enrichment analysis (GSEA) (Fig. 1g). Clusters 9 and 13 consist of BMPC expressing HLA-DR, a hallmark of recent generation from activated B cells (Fig. 1d). They represent proliferating plasmablasts (cluster 13) and newly generated plasma cells (cluster 9), with PD-1 signalling GSEA indicating their recent interaction with PD-1 expressing T cells.(Fig. 1g). BMPC of these two clusters also show GSEA characteristic of high oxidative phosphorylation and translational activity (Fig. 1g). Finally, clusters 11 and 12 are BMPC expressing heat shock genes and *NR4A1* (Nur77), respectively, (Fig. 1d) indicative of cellular stress. Nur77 has been described as an antagonist of Bcl-family members and inducer of apoptosis in myeloma cells[19], as well as being linked to B and T cell self-reactivity[20,21].

Overall, the increased *FAS* (CD95) and/or lower *BCL2* expression in $CD19^{high}$ clusters indicate that they might be transcriptionally more prone to succumb eventually to extrinsic and intrinsic apoptosis inducers (Supplementary Fig. 1d, e), while $CD19^{low}$ clusters may be more resilient. In support of this hypothesis, GSEA indicates that cells of clusters 1 and 6 show STAT3 and STAT5, and TNF receptor family signal transduction signatures, and they express IL5R as well as the TNF-family receptors TACI and BCMA (Fig. 1g, Supplementary Fig. 1e), the latter ones protecting plasma cells from anabolic stress [22–24]. Clusters 1 and 6 are also enriched in plasma cells expressing genes associated with hypoxia, a condition known to favour plasma cell survival in BM niches[25]. Finally, at the border of cluster 0 and 1 there is an enrichment of cells expressing genes associated with glycolysis, a metabolic condition crucial for plasma cell survival in BM niches[26] (Fig. 1g). In summary, analysis of phenotype and transcriptional profile of individual BMPC reveals a remarkable heterogeneity, even within the 10 clusters identified, which thus define clans of BMPC rather than homogeneous clusters.

BMPC have exclusive antibody repertoires

Consistent with their origin from distinct types of immune responses, the various clans of BMPC also express different repertoires of antigen-receptors. Overall, BMPC of the different clans are similar in diversity and not significantly oligoclonally expanded (Fig. 2a). The repertoires of clonal families of the different clans, defined by the combined heavy and light chain sequences (VDJ/VJ) of their BCR, do not overlap beyond what would be expected stochastically. An exception being the clonal overlap between clans 9 and 13, which suggests that these clans contain plasmablasts and newly generated plasma cells of the same recent or ongoing immune reaction (Fig. 2b). Mutations in the framework of CDR3 were more frequent in clans 0, 5, 8, i. e. the $CD19^{high}$ BMPC, as compared to the $CD19^{low}$ BMPC clans 1, 4 and 6 (Fig. 2c-f). In line with our previous findings[27], the mutation rates relate to the expression of CD19 and are lowest in cluster 1 and 4 which contain mostly $CD19^{low}$ plasma cells (Fig. 2e).

In order to sort out the distribution of antigen-specific cells of a given immune reaction into the different plasma cell clans, we analysed BMPC secreting antibodies specific for the receptor-binding domain (RBD) or full spike protein of SARS-CoV-2, or the tetanus toxoid (TT) C fragment. All BM samples were processed during the COVID-19 pandemic, resulting in the fact that the patients had either contact with

SARS-CoV-2 or had been vaccinated between 56 and 312 days prior to BM sampling (Supplementary Table 1). In all cases where serum could be analysed, patients had RBD- and spike-specific serum antibodies, as well as TT-specific serum antibodies (Supplementary Fig. 2a, Supplementary Table 1). Since most BMPC do not express antigen-receptors on their cell surface[28,29], direct isolation of viable antigen-specific BMPC for single cell sequencing was not possible. Rather, we identified them according to expression of VDJ and VJ genes expressed by individual RBD/spike- and TT-specific memory B cells and plasmablasts/plasma cells, isolated from the peripheral blood and BM of vaccinated healthy individuals (Supplementary Fig. 1a). As the VDJ/VJ germline genes of over a third of these clones were expressed by more than one of the analysed individuals, we designated them generically as “public” RBD/spike- and TT-specific clones, respectively (Supplementary Table 2). Of the 38235 BMPC analysed, 189 expressed spike-specific and 174 tetanus-specific public antigen receptors. These BMPC were present in clans 0, 1, 4, 5, 6, to lesser degree in 8 and 9, and very few in 11, 12 and 13 (Fig. 2g, h). Mutation rates were similar between spike- and tetanus-specific BMPC irrespective of the isotype they expressed, except for spike-specific IgA1 BMPC (Fig. 2i). These were significantly less mutated than tetanus-specific IgA1 BMPC. We identified clonal relations among the spike-specific BMPC (examples given in Fig. 2j and Supplementary Fig. 2b). These clones include the BMPC with the highest mutation rates of the BCR framework, are present in different clans (mostly in the $CD19^{high}$) and express different isotypes, including IgG2 and IgA2. In summary, tetanus- and SARS-CoV-2 spike-specific BMPC express somatically mutated antibodies and distribute to clans 0, 1, 4, 5, 6, 8 and 9, reflecting diverse or changing activating environments in the immune reaction in which they had been generated.

Differential distribution of antigen-specific BMPC within the $CD19^{low}$ and $CD19^{high}$ compartments

To overcome the limitations of low numbers of antigen-specific cells identified according to their expression of “public” VDJs, we also analysed SARS-CoV-2 spike-specific and TT-specific BMPC induced by SARS-CoV-2 vaccination by multiparametric flow cytometry. For a total of 20 BM samples (Supplementary Table 1) we identified both RBD of spike- and TT-specific plasma cells by intracellular staining with antigen, each labelled with two fluorescent dyes to exclude dye-specific PC (Fig. 3a, Supplementary Fig. 3a). The frequencies of RBD- and TT-specific BMPC did not significantly differ, with medians of 0.092% and 0.16%, respectively, of all BMPC analysed (Fig. 3b). These numbers are consistent with previous observations[30,31]. However, while the majority of RBD-specific plasma cells (67%) were $CD19^{high}$, the majority of TT-specific plasma cells (63%) were $CD19^{low}$ (Fig. 3c and Supplementary Fig. 3b). 75% of both RBD- and TT-specific BMPC expressed IgG, while 22% of RBD- and only 5% of TT-specific cells expressed IgA (Fig. 3d, Supplementary Fig. 3c). The remaining cells expressed IgM.

Considering the time elapsed after the third COVID-19 vaccination, frequencies of $CD19^{low}$ RBD-specific did increase over time, from about 20% at one month after the 3rd vaccination to more than 40% two months later (Fig. 3e). This could indicate that newly generated RBD-specific BMPC convert from

$CD19^{high}$ to $CD19^{low}$ over time, or that more and more $CD19^{low}$ PC are recruited to the BM and replace $CD19^{high}$ RBD-specific BMPC during the immune reaction to the vaccine, which is estimated to last 4 months or more[32].

BMPC heterogeneity reflects the different timings/stages of immune reactions

To follow up the dynamics of recruitment of PC to BM in a given immune reaction, we compared single cell transcriptomes of ASC exiting the immune reaction into the blood at various times after vaccination to the transcriptomes of BMPC. The longitudinal clinical study included 35 healthy individuals receiving different vaccines (Supplementary Table 3), namely the mRNA vaccine Comirnaty (SARS-CoV-2 spike, BioNTech/Pfizer, BNT), the viral vector-based vaccine Vaxzevria (SARS-CoV-2 spike, Oxford/AstraZeneca, AZ) and the mixed protein vaccine Boostrix (diphtheria toxoid, tetanus toxoid and pertussis toxoid, GlaxoSmithKline, DTP). To obtain single cell transcriptomes and BCR repertoires, viable $CD3^{-}CD14^{-}CD27^{high}CD38^{high}$ cells (Supplementary Fig. 4a) were isolated from peripheral blood 7 and 14 days after primary immunization (BNT, AZ), 7 days and 7 months after secondary BNT immunization and 7 days after third BNT vaccination (Fig. 4a). Circulating ASC from 7 days after primary vaccination of convalescent COVID-19 individuals, as well as 7 days and 6 months after boost with DTP vaccine were also isolated. Based on gene expression of *CD38, HLA-DMA* and *MKI67* (Fig. 4b) we classified the peripheral ASC into newly generated plasmablasts ($CD38^{high}$ $HLA\text{-}DMA^{high}$), proliferating plasmablasts ($MKI67^{+}$), and plasma cells ($CD38^{low}$ $HLA\text{-}DMA^{low}$)[30]. Cells of each stage express preferentially isotypes reflecting the cytokine milieu during their activation into antibody class switch recombination (Supplementary Fig. 4b). While the plasmablasts express mostly IgM, IgG1, IgG2, IgA1 and IgA2, the plasma cells express mainly IgA1. We defined gene signatures characteristic for the plasmablasts/plasma cells (ASC) isolated at different time points after vaccination (Supplementary Table 4) and projected these gene signatures onto the transcriptomes of the BMPC by GSEA (Fig. 4c, Supplementary Fig. 4c, d). 7 and 14 days after the first BNT or AZ vaccination, the signatures of circulating ASC mark clans 0, 1 and 4 of BMPC, both in terms of frequency and enrichment score (Fig. 4c, Supplementary Fig. 4c, d), with BNT delegating more PC into clans 1 and 4 than AZ, and AZ more into clan 9 than BNT. This difference is likely due to the fact that AZ also elicits an immune response against its adenovirus components (Supplementary Fig. 4e), as well as T-REx HEK293 proteins from virus production[33]. 7 days after the second BNT vaccination, BMPC of those that had received BNT 28 to 35 days before, again resembled BMPC of clan 1 and even more clan 4. Those primed with AZ, or infected with SARS-CoV-2 and boosted later with BNT, however, 7 days later had circulating ASC resembling BMPC of clans 0, 9, and 13. In an even more pronounced way, clans 0, 9, and 13 were expressing the signatures of ASC exiting into the blood 7 days after vaccination with DTP, a boost of established long term memory. In those vaccinated months after the second vaccination with a third dose of BNT, 7 days later the circulating ASC also shared signature gene expression with BMPC of clan 0, but also clans 4 and 5, i.e. IgA1 and IgA2 expressing $CD19^{low}$ BMPC.

In those vaccinees immunized twice with BNT, and in those boosted with DTP, we also analysed the circulating ASC 6 /7 months after vaccination. At this time we were still able to detect newly generated spike-specific ASC (Fig. 4d, e). Their signatures were mainly shared with BMPC of clans 0, 1, 5, 6 and 9 (Fig. 4c, Supplementary Fig. 4c, d). Peripheral ASC 6 months after DTP boost (DTP 6mo) resembled the ones obtained 7 months after BNT/BNT, with the exception of clan 1.

To determine whether the *in vivo* GSEA patterns also reflect the development of spike-specific antibodies, we tracked the maturation of public spike-specific B cell receptors over time after vaccination (Fig. 4d, Supplementary Table 2). We identified a total of 449 peripheral ASC expressing spike-specific public clones. Defining gene signatures of these cells identified at different time points after SARS-CoV-2 vaccination (Supplementary Table 5) and comparing them with BMPC by GSEA (Supplementary Fig. 4f, g) confirms the *in vivo* GSEA patterns (Fig. 4c).14 days after primary vaccination, when spike-specific serum antibodies became detectable (Supplementary Fig. 4h), the detected specific ASC of the BNT vaccinees were predominantly expressing IgG1, IgA1 and IgM (Fig. 4e). AZ vaccinees had predominantly IgA1, IgA2 and IgG1 spike-specific cells with higher somatic hypermutation. In both groups, after the second immunization, 3 and 12 weeks after the first, respectively, almost all identified spike-specific clones were of the IgG1 isotype. However, cells of the AZ/BNT vaccinees showed higher mutation rates. At 7 months after BNT/BNT vaccination, a uniform distribution across antibody classes was observed along with an increase in mutation rates, most likely resulting from a continued follicular germinal centre response[32]. 7 days after a third dose of BNT, we could detect public spike-specific BCRs of all different isotypes, with a predominance of IgG1 and IgA1 with increased mutation rates as compared to 14 days after primary and 7 days after secondary vaccination. Interestingly, convalescent individuals receiving just one dose of BNT showed predominantly IgG1 spike-specific BCRs with similar mutation rates as individuals receiving triple BNT vaccination (Fig. 4e).

Taken together, comparison of transcriptomes of ASC exiting the immune reaction, with those of established BMPC identify presumptive precursors of BMPC representing IL-6 and TGF-β-driven type III mucosal immune reactions (clusters 4 and 5), as well as IL-21 (clusters 0, 1 and 9), type II IFN (cluster 6) and type I IFN-driven (cluster 8) primary and secondary systemic immune reactions. $CD19^{low}$ BMPC of clan 1 predominantly originate from germinal centre reactions in the presence of IL-21, type I IFN and TGF-β. Those are generated within 7 days, mostly in primary immune reactions to BNT and AZ, and in the BNT/BNT vaccinees (Fig. 1, 4). $CD19^{high}$ clans 0, 6 and 9 represent BMPC derived from reactivation of memory B cells. 7 days after DTP boost, triple BNT vaccination and BNT vaccinated COVID-19 convalescents, nearly exclusively such plasmablasts exit the immune reaction. They manifest the imprinted immunological memory.

In conclusion, our data strongly suggest that $CD19^{low}$ clans of BMPC represent PC generated in germinal centre immune reactions, driven by follicular T helper cells and characterized by affinity maturation towards the inducing antigen. $CD19^{high}$ clans of BMPC represent PC generated by reactivation of already imprinted memory B cells in secondary immune reactions. In true recall reactions, i.e. DTP boost, triple

BNT, infection/BNT and AZ/BNT, we observe nearly exclusively generation of BMPC from memory B cells, locating to clans 0, 6, 8 and 9. Those clans differ with respect to the cytokines instructing immunoglobulin class switching of the activated B cells. Triple BNT also has the unique characteristic to induce IgA2 BMPC of $CD19^{low}$ clan 4, reflecting a prominent TGF-β driven follicular reaction. Since those BMPC also express the J chain, they qualify for secretion of secretory IgA2 and thus potentially a significant contribution to mucosal protection.

Methods

Human Donors

The recruitment of study subjects was conducted in accordance with the Ethics Committee of the Charité Universitätsmedizin Berlin in compliance with the Declaration of Helsinki (EA1/261/09). Informed consent was obtained from all bone marrow/peripheral blood donors included in the study. Bone marrow samples were obtained from 25 patients undergoing total hip arthroplasty without any underlying malignant or inflammatory disease (12 females and 13 males with a median age of 62 years, see Supplementary Table 1). Peripheral blood was obtain from 35 healthy volunteers at different time points after Comirnaty, Vaxzevria or Boostrix vaccination (16 females and 19 males with a median age of 32 years, see Supplementary Table 3).

Bone marrow plasma cell (BMPC) isolation

Bone marrow samples were fragmented and transferred to a 50mL tube where they were vortexed to separate cells from bone fragments. Samples were subsequently rinsed through a 70µM filter with PBS/1% BSA/5mM EDTA/2µg/mL actinomycin D to obtain a cell suspension. Plasma cells were enriched from bone marrow using StraightFrom Whole Blood and Bone Marrow CD138 MicroBeads and StraightFrom Whole Blood CD19 MicroBeads (Miltenyi Biotec) according to manufacturer's instructions. Enriched cells were incubated with Fc Blocking Reagent (Miltenyi Biotec) following manufacturer's instructions and subsequently stained for 30 min at 4°C with the following anti-human antibodies: CD3-VioBlue (BW264/56, Miltenyi Biotec, Cat. 130-113-133, 1:400), CD10-VioBlue (97C5, Miltenyi Biotec, Cat. 130-099-670, 1:11); CD14-VioBlue (TÜK4, Miltenyi Biotec, Cat. 130-113-152, 1:200); CD38-APC (HIT2, BioLegend, Cat. 303510, 1:25) and CD138-PE (44F9, Miltenyi Biotec, Cat. 130-119-840, 1:50) or CD3-VioBlue (BW264/56, Miltenyi Biotec, Cat. 130-113-133, 1:400), CD14-VioBlue (TÜK4, Miltenyi Biotec, Cat. 130-113-133, 1:200), CD27-APC-Cy7 (O323, BioLegend, Cat. 302816, 1:25), CD38-PerCP-Cy5.5 (HIT2, BD Biosciences, Cat. 551400, 1:100) and tetanus toxoid (AJ vaccines) coupled with Alexa Fluor 647 or Alexa Fluor 488 and SARS-Cov2 Spike Protein (Biotin, Miltenyi Biotec, Cat. 130-127-682) pre-incubated with streptavidin PE or streptavidin PE-Cy7 according to manufacturer's instructions. Simultaneously, cells were incubated with DNA barcoded antibodies for Cellular Indexing of Transcriptomes and Epitopes by Sequencing (CITE-seq, see antibody list). DAPI was added before sorting to allow dead cell exclusion. See Supplementary Fig. 1a for used gating strategies. All sortings were preformed using a MA900 Multi-

Application Cell Sorter (Sony Biotechnology). Cell counting was performed using a MACSQuant flow cytometer (Miltenyi Biotec). The sorted cells were further processed for single cell RNA sequencing.

Peripheral blood antibody-secreting cell (ASC) isolation

Cells were enriched from peripheral blood using StraightFrom Whole Blood CD19 and CD3 MicroBeads and StraightFrom Whole Blood and Bone Marrow CD138 MicroBeads (Miltenyi Biotec) according to manufacturer's instructions. 2µg/mL actinomycin D was added to the buffer used during the first centrifugation. Enriched cells were incubated with Fc Blocking Reagent (Miltenyi Biotec) following manufacturer's instructions and subsequently stained for 30 min at 4°C with the following anti-human antibodies: CD3-FITC (UCHT1, DRFZ in-house, 1:10), CD14-VioBlue (TÜK4, Miltenyi Biotec, Cat. 130-113-152, 1:200), CD27-PE (MT271, Miltenyi Biotec, Cat. 130-113-630, 1:100) and CD38-APC (HIT2, BioLegend, Cat. 303510, 1:25). Simultaneously, cells were incubated with DNA barcoded antibodies for Cellular Indexing of Transcriptomes and Epitopes by Sequencing (CITE-seq), which allowed identification of samples from different donors (see antibody list, hashtags). DAPI was added before sorting to allow dead cell exclusion. See Supplementary Fig. 4a for gating strategy. All sortings were performed using a MA900 Multi-Application Cell Sorter (Sony Biotechnology). Cell counting was performed using a MACSQuant flow cytometer (Miltenyi Biotec). The sorted cells were further processed for single cell RNA sequencing.

Single Cell RNA-library preparation and sequencing

Single cell suspensions were obtained by cell sorting and applied to the 10x Genomics workflow for cell capturing and scRNA gene expression (GEX), BCR and CITE-Seq library preparation using the Chromium Single Cell 5' Library & Gel Bead Kit version 2 for BMPC or version 1.1 for ASC, as well as the Single Cell 5' Feature Barcode Library Kit (10x Genomics). After cDNA amplification, the Cite-Seq libraries were prepared separately using the Dual Index Kit TN Set A for BMPC or the Single Index Kit N Set A for ASC. BCR target enrichment was performed using the Chromium Single Cell V(D)J Enrichment Kit for Human B cells. Final GEX and BCR libraries were obtained after fragmentation, adapter ligation and final Index PCR using the Dual Index Kit TT Set A for BMPC or the Single Index Kit T Set A for ASC. Qubit HS DNA assay kit (Life Technologies) was used for library quantification and fragment sizes were determined using the Fragment Analyzer with the HS NGS Fragment Kit (1-6000bp) (Agilent).

Sequencing was performed on a NextSeq2000 device (Illumina) applying the sequencing conditions recommended by 10x Genomics for libraries prepared with Next Gem Reagent Kits v2. NEXTSeq 1000/2000 P3 reagent kits (200 Cycles, Illumina) were used for 5' GEX and Cite-Seq libraries (for version 2, read1: 26nt, read2: 90nt, index1: 10nt, index2: 10nt; for version 1.1, read1: 26nt, read2: 98nt, index1: 8nt, index2: 0nt) and NEXTSeq 1000/2000 P3 reagent kits (300 Cycles, Illumina) were used for BCR libraries (for version 2, read1: 151nt, read2: 151nt, index1: 10nt, index2: 10nt., 2% PhiX spike-in, for version 1.1, read1: 151nt, read2: 151nt, index1: 8nt, index2: 0nt., 2% PhiX spike-in).

Single-cell transcriptome analysis

Raw sequence reads were processed using cellranger (version 5.0.0). Demultiplexing, mapping, detection of intact cells as well as quantification of gene expression was performed using cellranger's count pipeline in default parameter settings with refdata-cellranger-hg19-1.2.0 as reference and expected number of 3000 cells per sample. This led to 6206, 10818, 10707, 8189, 11020, 10800, 8394 and 9209 intact cells for 8 bone marrow samples. Cellranger's aggr was used to merge the libraries without size normalization and to perform a Uniform Manifold Approximation and Projection (UMAP). Loupe Browser (version 5, 10x Genomics) was used to identify and define bone marrow plasma cells (BMPC) by manual gating. Plasma cells defined clear regions with cells expressing *PRDM1*, *SDC1*, *XBP1* and *IRF4* genes. This led to 4051, 5505, 5661, 2222, 10988, 10730, 5528, 4556 plasma cells from each of the 8 bone marrow samples. The BMPC were further analysed in R (version 4.1.2) using the Seurat package (version 4.0.5)[34] and the cellranger's aggr output and the respective cellular barcodes. In particular, the transcriptome profiles of the bone marrow samples were read and plasma cells were extracted using Read10x, CreateSeuratObject and subset. To identify cells with similar transcriptional profiles among different sequencing libraries, sample specific batch effects were removed as described in FindIntegrationAnchors (Seurat) R Documentation. In particular, samples were analysed individually using SplitObject by LibraryID, NormalizeData with LogNormalization as normalization.method and scale.factor of 10,000, FindVariableFeatures with 2000 variable genes and vst as selection.method, ScaleData and finally RunPCA to compute 50 principle components for each sample. Next, common anchors were identified by FindIntegrationAnchors usind rpca as reduction, 2000 anchor.features and 1:30 dimensions and finally merged using IntegrateData. Based on the integrated data, a uniform manifold approximation and projection (UMAP) was computed using ScaleData, RunPCA to compute 50 principle components and RunUMAP using 1:30 dimensions. Transcriptionally similar clusters were identified by shared nearest neighbor (SNN) modularity optimization using FindNeighbors with pca as reduction and 1:30 dimensions as well as FindClusters with resolutions ranging from 0.1 to 1.0 in 0.1 increments using FindCluster. Further analyses were based on non-integrated, log normalized values represented as ln (10,000 * UMIsGene) /UMIsTotal + 1) and the above integrations-based clusters and UMAP. By visual inspection of the percentage of mitochondrial genes, UMI counts, number of identified genes as well as expression of typical marker genes projected on the UMAP, clustering with a resolution of 0.5 was judged to best reflect the transcriptional community structure. Clusters comprising low quality cells as well as clusters comprising contaminations were not considered in further analyses.

The single-cell transcriptome analysis of ASC were performed in accordance to the BMPC analysis. In particular, 34 libraries of pooled samples from 35 subjects at different time-points (see Supplementary Table 3) were demultiplexed and mapped, intact cells were detected, and gene expression was quantified by cellranger's count pipeline and merged by cellranger aggr. This led to 32162 and 32506 intact cells at d7 and d14 after Comirnaty 1st dose of (BNT d7, d14), respectively; 42047 and 26339 cells at d7 and 7 months after Comirnaty 2nd dose (BNT/BNT d7, 7mo), respectively; 32860 cells at d7 after Comirnaty 3rd dose (BNT/BNT/BNT d7); 28282 and 24622 cells at d7 and d14 after Vaxzevria 1st dose (AZ d7, d14), respectively; 16567 cells at d7 after Comirnaty 2nd dose (1st dose Vaxzevria, AZ/BNT d7); 21524 cells at d7 after 1st Comirnaty dose of donors recovered from a SARS-Cov-2 infection (COVID/BNT d7); and

29875 and 22811 cells at d7 and 6mo after Boostrix boost (DTP d7, 6mo), respectively. Libraries were merged by cell ranger's aggr. Loupe Browser (version 5, 10x Genomics) was used to identify and define ASC by manual gating. ASC defined clear regions with cells expressing higher levels of *PRDM1*, *CD27* and *CD38* genes. This led to 4462 and 5762 ASC at d7 and d14 after Comirnaty 1st dose of (BNT d7, d14), respectively; 5983 and 4169 ASC at d7 and 7 months after Comirnaty 2nd dose (BNT/BNT d7, 7mo), respectively; 6036 ASC at d7 after Comirnaty 3rd dose (BNT/BNT/BNT d7); 8540 and 2143 ASC at d7 and d14 after Vaxzevria 1st dose (AZ d7, d14), respectively; 2969 ASC at d7 after Comirnaty 2nd dose (1st dose Vaxzevria, AZ/BNT d7); 5586 ASC at d7 after 1st Comirnaty dose of donors recovered from a SARS-Cov-2 infection (COVID/BNT d7); and 5679 and 3742 ASC at d7 and 6mo after Boostrix boost (DTP d7, 6mo), respectively. ASC were further analysed with the Seurat package R-package using the cellranger's aggr output and the respective cellular barcodes. UMAP was performed by removal of library and donor specific batch effects using the Seurat's integration. Visualized is the log normalized gene expression of non-integrated data.

Single-cell immune profiling

Raw sequence reads were processed using cellranger (version 5.0.0). Vdj was used in default parameter settings for demultiplexing and assembly of the B cell receptor sequences using refdata-cellranger-vdj-GRCh38-alts-ensembl-2.0.0 as reference. The cellranger output was further analysed in R (version 4.1.2) using the Seurat package (version 4.0.5)[34].

B cell receptor isotypes and receptor sequences were assigned to the corresponding cells in the single cell transcriptome analysis by identical cellular barcodes. In case of multiple contigs, the most abundant, productive and fully sequenced contig for the heavy and light BCR chain was used. This led to the annotation of 95% (3856), 90% (4954), 90% (5097), 94% (2081), 87% (9551), 85% (9105), 91% (5,032) and 93% (4237) plasma cells for the 8 BM samples; 69% (3060) and 67% (3860) ASC at d7 and d14 after Comirnaty 1st dose of (BNT d7, d14), respectively; 65% (3893) and 66% (2762) ASC at d7 and 7 months after Comirnaty 2nd dose (BNT/BNT d7, 7mo), respectively; 70% (4248) ASC at d7 after Comirnaty 3rd dose (BNT/BNT/BNT d7); 53% (4525) and 64% (1364) ASC at d7 and d14 after Vaxzevria 1st dose (AZ d7, d14), respectively; 65% (1931) ASC at d7 after Comirnaty 2nd dose (1st dose Vaxzevria, AZ/BNT d7); 61% (3405) ASC at d7 after 1st Comirnaty dose of donors recovered from a SARS-Cov-2 infection (COVID/BNT d7); and 69% (3938) ASC at d7 after Boostrix boost (DTP d7). Samples from 6 months after Boostrix boost were not immune profiled. The high-confidence contig sequences with an associated transcriptional profile were reanalysed using the HighV-QUEST at IMGT web portal for immunoglobulin (IMGT) to retrieve the germline sequence between of the FR1-CDR1-FR2-CDR2-FR2, the V-, J- and D-gene information as well as the nucleotide and amino acid CDR3 sequence. The HighV-QUEST output, in particular the IMGT-gapped-nt-sequences and V-REGION-mutation-and-AA-change-table were used to reverse engineer the gapped germline FR1-CDR1-FR2-CDR2-FR2 sequence. A clonal family of a BCR receptor was defined by the gapped germline FR1-CDR1-FR2-CDR2-FR2 sequence, the length of the CDR3 sequence and used VJ-genes in both the heavy and light chain. The clonal family annotation was used to compute the diversity, Simson Diversity Index as well as the overlap table. Significance of an overlap was

evaluated by 1000 permutation of the clonal family annotation of the cells. Mutation counts in framework regions (FR1, FR2, FR3) were taken from V-REGION-nt-mutation-statistics of the HighV-QUEST output. Mutation rates were defined as the sum of the estimated mutation counts in the heavy and light chain normalized to the length of the corresponding nt sequence length.

The clonal family of spike- and tetanus-specific public clones were derived from BCR sequencing of spike- and tetanus-specific B cells isolated with either fluorophore-coupled RBD/Spike protein of SARS-CoV2 or tetanus toxoid after vaccination of healthy subjects with Comirnaty or Boostrix vaccines. In particular, raw sequence reads from BCR-sequencing were processed using cellranger vdj pipeline as described above. The contig sequences were reanalysed using the HighV-QUEST at IMGT web portal for immunoglobulin (IMGT) to retrieve the germline sequence between of the FR1-CDR1-FR2-CDR2-FR2, the V-, J- and D-gene information as well as the nucleotide and amino acid CDR3 sequence. Solely contig pairs for the heavy and light chain were considered. Unpaired contigs, that is contigs without a corresponding contig with the same cellular barcode, were removed from further analyses. In case of multiple contigs for the same cellular barcode, the most abundant, productive and fully sequenced contig for the heavy and light BCR chain were used. The HighV-QUEST output was used to define public clonal families as described above. Putative spike- and tetanus-specific clones in BMPC and ASC samples were defined by clonal families found in spike- and tetanus-specific public clones. Mutation trees of public clonal families were based on the FR1-CDR1-FR2-CDR2-FR2 sequences. In particular, the FR1-FR3 sequences of the BMPC clones with clonal families found in spike- and tetanus-specific public clones were extracted, the sequence of the heavy and light chain concatenated, and a minimum spanning tree was constructed for each family using GLaMST (PMID: 32900378) using the germline FR1-CDR1-FR2-CDR2-FR2 sequence as root. Solely clonal families with clones found in at least three different clusters of BMPC single-cell transcriptome analysis were analysed.

Gene Set Enrichment Analysis (GSEA)

GSEA was performed for each cell based on the difference to the mean of log normalized expression values of all cells in the analysed set as pre-ranked list and 1000 randomizations (PMID: 16199517, PMID: 12808457). Significant up- or downregulation was defined by a FDR $\leq$ 0.50 and normalized p-value < 0.05 43. For visualization, NES for significant cells were plotted. The GSEA was performed for indicated cells using hallmark gene sets (PMID: 26771021), REACTOME (PMID: 29145629) and KEGG (PMID: 10592173). Hallmark gene sets, REACTOME and KEGG were obtained from the MSigDB Collections (PMID: 26771021) as well as time-specific gene sets (ASC signature gene set) and time-specific-spike-specific gene sets (SPIKE signature gene set) from the ASC analysis as defined by marker genes for different time points after vaccination (Supplementary Table 4, 5). For the ASC signature gene set samples at day 7 and day 14 after first Comirnaty vaccination, day 7 and 7 months after second Comirnaty vaccination, day 7 after third Comirnaty vaccination, day 7 and day 14 after Vaxzevria vaccination, day 7 after second Comirnaty vaccination (heterologous), day 7 after Comirnaty vaccination from donors recovered from a SARS-Cov-2 infection, as well as samples at day 7 and 6 months after vaccination with Boostrix, genes with an Area under the ROC Curve greater than 0.6 and an adjusted p-

value < = 0.05 (Mann Whitney U Test) were defined as marker genes. Solely expression values greater than 0 were considered. Likewise, the time-specific-spike-specific marker gene sets were derived from a ROC-analysis. Genes with an Area under the ROC Curve greater than 0.65 and an adjusted p-value < = 0.05 (Mann Whitney U Test) were defined as marker genes. To increase the statistical power, the expression value of not expressed genes was set to 0.

The GSEA results were visualized by density plot on UMAPs as well as on violin plots of the NES score of significant enriched cells with a positive NES score. Differences in positive NES scores were evaluated using the Mann Whitney U Test.

Bone marrow mononuclear cells flow cytometry analysis

Bone marrow mononuclear cells were enriched by density gradient centrifugation over Ficoll-Paque PLUS (GE Healthcare Bio-Sciences), as described previously[27]. Briefly, samples were fragmented, rinsed with PBS/0.5%BSA/EDTA (PBE) (Miltenyi Biotech). The collected BM mononuclear cells were filtered with a 70 µm cell strainer (BD Biosciences), and then washed twice with PBE for staining.

All flow cytometry analyses were performed using a BD FACS Fortessa (BD Biosciences). To ensure comparable mean fluorescence intensities over time of the analyses, Cytometer Setup and Tracking beads (BD Biosciences) and Rainbow Calibration Particles (BD Biosciences) were used. For staining, LIVE/DEAD Fixable Blue Dead Cell Stain Kit (ThermoFisher Scientific) was used to exclude dead cells according to the manufacturer's protocol. BM cells were surface-stained for 30 min at 4°C with the following anti-human antibodies: CD138-BUV737 (MI15, BD Biosciences, Cat. 564393, 1:20), CD14-BUV395 (M5E2, BD Biosciences, Cat. 740286, 1:50), CD3-BUV395 (UCHT1, BD Biosciences, Cat. 563546, 1:50), CD27-BV786 (L128, BD Biosciences, Cat. 563328, 1:50), CD19-BV711 (SJ25C1, BD Biosciences, Cat. 563038, 1:50), CD20-BV510 (2H7, BioLegend, Cat. 302340, 1:50), IgD-PE/Dazzle594 (IA6-2, BioLegend, Cat. 348240, 1:500), CD38-APC-Cy7 (HIT2, BioLegend, Cat. 303534, 1:500), HLA-DR- PE (Tü36, BD Biosciences, Cat. 555561, 1:10), CD56-BV421 (HCD56, BioLegend, Cat. 318328, 1:25) diluted in Brilliant Stain buffer (BD Horizon). Cells were washed twice with PBE, fixed for 20 min at 4°C using Fixation/Permeabilization Solution Kit (BD Cytofix/Cytoperm™ Plus) and washed twice with perm/wash buffer. Cells were then stained intracellularly for 30 min 4°C with recombinant purified RBD (DAGC149, Creative Diagnostics, New York, USA) and TT (AJ vaccines) which were coupled with either Alexa Fluor 647 or Alexa Fluor 488 to identify antigen-specific cells as previously described[35,36], and with anti-human antibodies to detect expressed isotypes: IgA-biotin (G20-359, BD Biosciences, Cat. 555884, 1:50), IgG-PE-Cy7 (G18-145, BD Biosciences, Cat. 561298, 1:500), IgM-BV421 (G20-127, BD Biosciences, Cat. 562618, 1:100). Double-positive cells were considered as antigen-specific cells (See Fig. 3a). Flow cytometric data were analysed by FlowJo software 10.7.1 (TreeStar).

One-tail spearman's correlation coefficients were estimated to assess the relationship between the frequencies of $CD19^-$ frequency of antigen-specific BMPCs and the time since the 3rd SARS-CoV2 vaccination. Mann-Whitney U test was used for comparison of two groups and Kruskal-Wallis with Dunn

´s post-test was used for multiple comparisons. All statistical analyses were conducted using Prism version 9 (GraphPad), and P values of less than 0.05 were considered significant.

Enzyme-linked immunosorbent assay for the detection of serum specific antibody titers on patients undergoing hip replacement surgery

To determine the tetanus toxoid and SARS-CoV2 RBD-specific antibody titers, 96-well plates were coated overnight with 0.5 µg/ml of either tetanus toxoid (AJ vaccines) or SARS-CoV-2 (2019-nCoV) Spike RBD-His recombinant protein (Sino biological, Cat. 40592-V08B-100). Coated plates were washed, blocked for 1 hour with PBS 5% BSA and incubated overnight at 4°C with serial dilutions of sera. Specific IgA antibodies were detected using anti-human IgA-Biotin (Southern Biotech, Cat. 2050-08) followed by streptavidin-HRP (Invitrogen, Cat. N100) and specific IgG antibodies were detected using anti-human IgG-HRP (Southern Biotech, Cat. 2040-05). Detection antibody incubation was performed at room temperature for 1 hour. After washing 5 times with PBST, Tetramethylbenzidine (TMB) Substrate (Invitrogen, Cat. 88-7324-88) was added. The reaction was stopped by addition of 2N H_2SO_4 (Sigma-Aldrich: Cat. 84736). Optical densities were measured on Spectramax (Molecular devices). Optical densities were measured on Spectramax plus 384(Molecular devices). OD values were further plotted against respective sample dilutions and areas under the curve (AUC) were quantified using Graphpad Prism 9.3.1.

Flow cytometric assay for the detection of serum specific antibody titers on patients undergoing hip replacement surgery

HEK293T cells (ATCC CRL-3216) were transfected with a plasmid expressing wild-type SARS-CoV-2 S protein. Next day, the proportion of transfected cells was determined by staining with anti-SARS-CoV-2 Spike Glycoprotein S1 antibody (clone: CR3022, Abcam, Cat. ab273073) for 30 min, wash cells once with PBS/0.2% BSA and subsequent staining with goat anti-human IgG-Alexa647 (Southern Biotech, Cat. 2014-31). Further transfected cells were collected and incubated with sera for 30 min, washed twice with PBS/BSA and stained with goat anti-human IgG-Alexa647 (Southern Biotech, Cat. 2014-31) and anti-human IgA FITC (Sothern Biotech, Cat. 2052-02). Cells were washed with PBS/ 0.2% BSA and either measured directly, dead cell exclusion by DAPI or stained for dead cells with Zombie Violet™ (Biolegend, Cat. 423113) in PBS for 5 min at room temperature and fixed in 4% paraformaldehyde solution overnight at 4°C. Samples were acquired on a FACSCanto (BD Biosciences) or a MACS Quant 16 (Miltenyi) and analysed using FlowJo v10 (Tree Star Inc.) analysis software. In the respective fluorescent channels, geometric mean of fluorescent intensity (MFI) Spike expressing cells and non-expressing cells was quantified and ΔMFI = MFI (S+)-MFI (S-) for IgG and IgA was determined. ΔMFI values were further plotted against respective serum dilutions and AUC were quantified using Graphpad Prism 9.3.1.

Enzyme-linked immunosorbent assay for the detection of serum specific antibody titers on vaccinated individuals

The amount of SARS-CoV-2 spike RBD-specific antibodies was quantified using an in-house ELISA described previously[37]. Purified RBD protein was used for coating at a concentration of 5 µg/ml and 50 µl per well in a 96-well microtiter plate (Costar 3590, Corning Incorporated, Kennebunk, USA). For the ChAd-Y25 titer, the same ELISA approach was used and 5 x 108 viral particles/well of the Vaxzevria vaccine (AstraZeneca, Oxford) was used for coating. After overnight coating at 4°C, 230 µl of 10% FCS in PBS per well was used for blocking. Blocking was performed for 1 hour at RT. Plates were washed four times with PBS-T (PBS containing 0.05% Tween). 50 µl of the in blocking buffer 1:100 diluted sera were incubated in the wells for 1.5 h. An HRP-linked anti-human IgG antibody (Cytiva, Cat. NA933-1ML, Dassel, Germany) at a dilution of 1:3000 was used as a secondary antibody and incubated for 1.5 h on the plates. After washing five times, plates were developed for 5 min with 100 µl TMB solution (eBioscience, San Diego, USA) and stopped with the same volume of 1 N sulphuric acid. Absorbance was measured directly at 450 m on an Infinite M1000 reader (Tecan Group, Männedorf, Switzerland).

Antibody list

Antibody	*Clone*	*Conjugate*	*Source*	*Cat No*
CD3	BW264/56	VioBlue	Miltenyi Biotec	130-113-133
CD3	UCHT1	FITC	DRFZ in-house	
CD3	UCHT1	BUV395	BD Biosciences	563546
CD10	97C5	VioBlue	Miltenyi Biotec	130-099-670
CD14	TÜK4	VioBlue	Miltenyi Biotec	130-113-152
CD14	M5E2	BUV395	BD Biosciences	740286
CD19	SJ25C1	BV711	BD Biosciences	563038
CD20	2H7	BV510	BioLegend	302340
CD27	MT271	PE	Miltenyi Biotec	130-113-630
CD27	O323	APC-Cy7	BioLegend	302816
CD27	L128	BV786	BD Biosciences	563328
CD38	HIT2	APC	BioLegend	303510
CD38	HIT2	APC-Cy7	BioLegend	303534
CD38	HIT2	PerCP-Cy5.5	BioLegend	551400
CD56	HCD56	BV421	BioLegend	318328
CD138	44F9	PE	Miltenyi Biotec	130-119-840
CD138	MI15	BUV737	BD Biosciences	564393
HLA-DR	Tü36	PE	BD Biosciences	555561
IgA	G20-359	Biotin	BD Biosciences	555884
IgA	Polyclonal	FITC	Southern Biotech	2052-02
IgD	IA6-2	PE/Dazzle594	BioLegend	348240
IgG	G18-145	PE-Cy7	BD Biosciences	561298
IgG	Polyclonal	Alexa647	Southern Biotech	2014-31
IgM	G20-127	BV421	BD Biosciences	562618
CD11c	S-HCL-3	TACGCCTATAACTTG	BioLegend	371521
CD19	HIB19	CTGGGCAATTACTCG	BioLegend	302265
CD20	2H7	TTCTGGGTCCCTAGA	BioLegend	302363
CD21	Bu32	AACCTAGTAGTTCGG	BioLegend	354923

Antibody	*Clone*	*Conjugate*	*Source*	*Cat No*
CD23	EBVCS-5	TCTGTATAACCGTCT	BioLegend	338525
CD27	O323	GCACTCCTGCATGTA	BioLegend	302853
CD28	CD28.2	TGAGAACGACCCTAA	BioLegend	302963
CD29	TS2/16	GTATTCCCTCAGTCA	BioLegend	303029
CD38	HIT2	TGTACCCGCTTGTGA	BioLegend	303543
CD40	5C3	CTCAGATGGAGTATG	BioLegend	334348
CD44	IM7	TGGCTTCAGGTCCTA	BioLegend	103063
CD45	HI30	TGCAATTACCCGGAT	BioLegend	304068
CD49d	9F10	CCATTCAACTTCCGG	BioLegend	304345
CD49f	GoH3	TTCCGAGGATGATCT	BioLegend	313635
CD56	QA17A16	TTCGCCGCATTGAGT	BioLegend	392425
CD62L	DREG-56	GTCCCTGCAACTTGA	BioLegend	304851
CD66b	6/40c	AGCTGTAAGTTTCGG	BioLegend	392909
CD71	CY1G4	CCGTGTTCCTCATTA	BioLegend	334125
CD73	AD2	CAGTTCCTCAGTTCG	BioLegend	344031
CD79b	CB3-1	ATTCTTCAACCGAAG	BioLegend	341417
CD80	2D10	ACGAATCAATCTGTG	BioLegend	305243
CD86	IT2.2	GTCTTTGTCAGTGCA	BioLegend	305447
CD95	DX2	CCAGCTCATTAGAGC	BioLegend	305651
CD98	MEM-108	GCACCAACAGCCATT	BioLegend	315607
CD107a	H4A3	CAGCCCACTGCAATA	BioLegend	328649
CD138	DL-101	GTATAGACCAAAGCC	BioLegend	352327
CD183	G025H7	GCGATGGTAGATTAT	BioLegend	353747
CD184	12G5	TCAGGTCCTTTCAAC	BioLegend	306533
CD185	J252D4	AATTCAACCGTCGCC	BioLegend	356939
CD268	11C1	CGAAGTCGATCCGTA	BioLegend	316927
CD269	19F2	CAGATGATCCACCAT	BioLegend	357523
CD273	24F.10C12	TCAACGCTTGGCTAG	BioLegend	329621

Antibody	*Clone*	*Conjugate*	*Source*	*Cat No*
CD274	29E.2A3	GTTGTCCGACAATAC	BioLegend	329751
CD319	162.1	AGTATGCCATGTCTT	BioLegend	331823
HLA-DR	L243	AATAGCGAGCAAGTA	BioLegend	307663
IgD	IA6-2	CAGTCTCCGTAGAGT	BioLegend	348245
IgM	MHM-88	TAGCGAGCCCGTATA	BioLegend	314547
Integrin β7	FIB504	TCCTTGGATGTACCG	BioLegend	321229
Hashtag 1	LNH-94; 2M2	GTCAACTCTTTAGCG	BioLegend	394661
Hashtag 2	LNH-94; 2M2	TGATGGCCTATTGGG	BioLegend	394663
Hashtag 3	LNH-94; 2M2	TTCCGCCTCTCTTTG	BioLegend	394665
Hashtag 4	LNH-94; 2M2	AGTAAGTTCAGCGTA	BioLegend	394667
Hashtag 5	LNH-94; 2M2	AAGTATCGTTTCGCA	BioLegend	394669
Hashtag 6	LNH-94; 2M2	GGTTGCCAGATGTCA	BioLegend	394671
Hashtag 7	LNH-94; 2M2	TGTCTTTCCTGCCAG	BioLegend	394673
Hashtag 8	LNH-94; 2M2	CTCCTCTGCAATTAC	BioLegend	394675
Hashtag 9	LNH-94; 2M2	CAGTAGTCACGGTCA	BioLegend	394677
Hashtag 10	LNH-94; 2M2	ATTGACCCGCGTTAG	BioLegend	394679
IgA	Polyclonal	Biotin	Southern Biotech	2050-08
IgG	Polyclonal	HRP	Southern Biotech	2040-05
IgG	Polyclonal	HRP	Cytiva	NA933-1ML

Declarations

DATA AVAILABILITY

Next Generation Sequencing data sets generated and analysed during the current study are available in the GEO repository under accession number GSEXXX. [Comment to the editor/review: Data being uploaded]. Source data are provided with this paper. All other data that support the findings of this study are available on request from the corresponding author [M.F.M.] or the special correspondence for bioinformatics [P. D.].

CODE AVAILABILITY

The software used in this study is open source.

Cellranger from 10x genomics: https://support.10xgenomics.com/single-cell-gene-expression/software/downloads/latest

Seurat packages 4.1.1: https://cloud.r-project.org/web/packages/Seurat/index.html

Used scripts are available upon request.

ACKNOWLEDGEMENTS

The authors are most grateful to the patients for their consent in participating in this study. We would like to thank Antje Blankenstein, Johanna Penzlin and Simon Reinke from the BCRT Cell Harvesting Laboratory and the Charité Orthopedics Surgery Department for provision of samples. We also thank Jenny Kirsch and Toralf Kaiser from the DRFZ Flow Cytometry Core Facility for support in cell sorting. This work was kindly supported by the following entities: the German Research Foundation (DFG) through the grants LI3540/1-1, Do491/8-1/2 (SPP Immunobone) and Do491/10-1, 11-1 to T.D., TRR130/TP24 to H.E.M. and T.D, TRR130/TP16 to A.R. and TRR241/A04 to A.K.; the Federal Ministry of Education and Research (BMBF) with financing of the projects TReAT and CONAN; the state of Berlin and the “European Regional Development Fund” through the grant ERDF 2014-2020, EFRE 1.8/11, to M.F.M.; the Leibniz Association through the Leibniz Collaborative Excellence, TargArt project to M.F.M.; the Berlin senate through the financing of the project: “Modulation of the mucosal immune response to prevent severe COVID-19 disease progression by commensal bacteria or vaccination” to M.F.M.; the Berlin Institute of Health through the Starting Grant Multi-Omics Characterization of SARS-CoV-2 infection, Project 6 “Identifying immunological targets in COVID-19” to M.F.M.; the Russian Ministry of Science and Higher Education of the Russian Federation through the grant 075-15-2019-1660 and the Russian Foundation for Basic Research through the grant no. 17-00-00268 to A.K.

AUTHOR CONTRIBUTIONS

Conceptualization: A.R., T.D., M.F.M.;

Methodology: M.F.G., Y.C., P.D., H.R.A., F.S., G.M.G., A.C.L.;

Software: P.D., F.H., F.S.;

Validation: M.F.G., A.C.L., M.F.M.;

Formal analysis: P.D., F.H., F.S.;

Investigation: M.F.G., Y.C., H.R.A., G.M.G., A.L.S., A.N., A.W., M.B., J.C.R., K.L., S.H., V.D.D.;

Resources: S.H., C.H., Q.C., M.W., H.E.M., E.V.S.;

Data curation: M.F.G.; P.D., M.F.M.;

Writing - original draft: M.F.G., M.F.M.;

Writing - Review & editing: M.F.G., Y.C., F.M., A.C.L., A.R., T.D.;

Visualization: M.F.G., Y.C., P.D., F.H., F.S.;

Supervision: E.H., M.M., A.C.L., A.K., C.P., A.R., T.D., M.F.M.;

Project administration: T.D., M.F.M.;

Funding acquisition: A.R., T.D., M.F.M.

COMPETING INTERESTS

The authors declare no competing interests.

References

1. Radbruch, A. *et al.* Competence and competition: the challenge of becoming a long-lived plasma cell. Nat Rev Immunol **6**, 741–750 (2006). https://doi.org:10.1038/nri1886
2. Manz, R. A., Thiel, A. & Radbruch, A. Lifetime of plasma cells in the bone marrow. Nature **388**, 133–134 (1997). https://doi.org:10.1038/40540
3. Slifka, M. K., Antia, R., Whitmire, J. K. & Ahmed, R. Humoral immunity due to long-lived plasma cells. Immunity **8**, 363–372 (1998). https://doi.org:10.1016/s1074-7613(00)80541-5
4. Turner, J. S. *et al.* SARS-CoV-2 infection induces long-lived bone marrow plasma cells in humans. Nature **595**, 421–425 (2021). https://doi.org:10.1038/s41586-021-03647-4
5. Kim, W. *et al.* Germinal centre-driven maturation of B cell response to mRNA vaccination. Nature **604**, 141–145 (2022). https://doi.org:10.1038/s41586-022-04527-1
6. Amanna, I. J., Carlson, N. E. & Slifka, M. K. Duration of humoral immunity to common viral and vaccine antigens. N Engl J Med **357**, 1903–1915 (2007). https://doi.org:10.1056/NEJMoa066092
7. Arce, S. *et al.* CD38 low IgG-secreting cells are precursors of various CD38 high-expressing plasma cell populations. J Leukoc Biol **75**, 1022–1028 (2004). https://doi.org:10.1189/jlb.0603279
8. Wiedemann, A. *et al.* Human IgA-Expressing Bone Marrow Plasma Cells Characteristically Upregulate Programmed Cell Death Protein-1 Upon B Cell Receptor Stimulation. Front Immunol **11**, 628923 (2020). https://doi.org:10.3389/fimmu.2020.628923
9. Dang, V. D. *et al.* CD39 and CD326 Are Bona Fide Markers of Murine and Human Plasma Cells and Identify a Bone Marrow Specific Plasma Cell Subpopulation in Lupus. Front Immunol **13**, 873217 (2022). https://doi.org:10.3389/fimmu.2022.873217
10. Bortnick, A. *et al.* Long-lived bone marrow plasma cells are induced early in response to T cell-independent or T cell-dependent antigens. J Immunol **188**, 5389–5396 (2012). https://doi.org:10.4049/jimmunol.1102808

11. Weisel, F. J., Zuccarino-Catania, G. V., Chikina, M. & Shlomchik, M. J. A Temporal Switch in the Germinal Center Determines Differential Output of Memory B and Plasma Cells. Immunity **44**, 116–130 (2016). https://doi.org:10.1016/j.immuni.2015.12.004
12. Robinson, M. J. *et al.* Long-lived plasma cells accumulate in the bone marrow at a constant rate from early in an immune response. Sci Immunol **7**, eabm8389 (2022). https://doi.org:10.1126/sciimmunol.abm8389
13. Fujieda, S., Saxon, A. & Zhang, K. Direct evidence that gamma 1 and gamma 3 switching in human B cells is interleukin-10 dependent. Mol Immunol **33**, 1335–1343 (1996). https://doi.org:10.1016/s0161-5890(96)00092-2
14. Pene, J. *et al.* Cutting edge: IL-21 is a switch factor for the production of IgG1 and IgG3 by human B cells. J Immunol **172**, 5154–5157 (2004). https://doi.org:10.4049/jimmunol.172.9.5154
15. Islam, K. B., Nilsson, L., Sideras, P., Hammarstrom, L. & Smith, C. I. TGF-beta 1 induces germ-line transcripts of both IgA subclasses in human B lymphocytes. Int Immunol **3**, 1099–1106 (1991). https://doi.org:10.1093/intimm/3.11.1099
16. Kitani, A. & Strober, W. Regulation of C gamma subclass germ-line transcripts in human peripheral blood B cells. J Immunol **151**, 3478–3488 (1993).
17. Becht, E. *et al.* Dimensionality reduction for visualizing single-cell data using UMAP. Nat Biotechnol (2018). https://doi.org:10.1038/nbt.4314
18. Mei, H. E. *et al.* Blood-borne human plasma cells in steady state are derived from mucosal immune responses. Blood **113**, 2461–2469 (2009). https://doi.org:10.1182/blood-2008-04-153544
19. Luciano, F. *et al.* Nur77 converts phenotype of Bcl-B, an antiapoptotic protein expressed in plasma cells and myeloma. Blood **109**, 3849–3855 (2007). https://doi.org:10.1182/blood-2006-11-056879
20. Liebmann, M. *et al.* Nur77 serves as a molecular brake of the metabolic switch during T cell activation to restrict autoimmunity. Proc Natl Acad Sci U S A **115**, E8017-E8026 (2018). https://doi.org:10.1073/pnas.1721049115
21. Tan, C. *et al.* Nur77 Links Chronic Antigen Stimulation to B Cell Tolerance by Restricting the Survival of Self-Reactive B Cells in the Periphery. J Immunol **202**, 2907–2923 (2019). https://doi.org:10.4049/jimmunol.1801565
22. Cornelis, R. *et al.* Stromal Cell-Contact Dependent PI3K and APRIL Induced NF-kappaB Signaling Prevent Mitochondrial- and ER Stress Induced Death of Memory Plasma Cells. Cell Rep **32**, 107982 (2020). https://doi.org:10.1016/j.celrep.2020.107982
23. Cornelis, R., Chang, H. D. & Radbruch, A. Keeping up with the stress of antibody production: BAFF and APRIL maintain memory plasma cells. Curr Opin Immunol **71**, 97–102 (2021). https://doi.org:10.1016/j.coi.2021.06.012
24. Burt, P. *et al.* Data-Driven Mathematical Model of Apoptosis Regulation in Memory Plasma Cells. Cells **11** (2022). https://doi.org:10.3390/cells11091547
25. Nguyen, D. C. *et al.* Author Correction: Factors of the bone marrow microniche that support human plasma cell survival and immunoglobulin secretion. Nat Commun **10**, 372 (2019).

https://doi.org:10.1038/s41467-019-08400-0

26. Lam, W. Y. *et al.* Mitochondrial Pyruvate Import Promotes Long-Term Survival of Antibody-Secreting Plasma Cells. Immunity **45**, 60–73 (2016). https://doi.org:10.1016/j.immuni.2016.06.011
27. Mei, H. E. *et al.* A unique population of IgG-expressing plasma cells lacking CD19 is enriched in human bone marrow. Blood **125**, 1739–1748 (2015). https://doi.org:10.1182/blood-2014-02-555169
28. Pinto, D. *et al.* A functional BCR in human IgA and IgM plasma cells. Blood **121**, 4110–4114 (2013). https://doi.org:10.1182/blood-2012-09-459289
29. Hibi, T. & Dosch, H. M. Limiting dilution analysis of the B cell compartment in human bone marrow. Eur J Immunol **16**, 139–145 (1986). https://doi.org:10.1002/eji.1830160206
30. Odendahl, M. *et al.* Generation of migratory antigen-specific plasma blasts and mobilization of resident plasma cells in a secondary immune response. Blood **105**, 1614–1621 (2005). https://doi.org:10.1182/blood-2004-07-2507
31. Giesecke, C. *et al.* Tissue distribution and dependence of responsiveness of human antigen-specific memory B cells. J Immunol **192**, 3091–3100 (2014). https://doi.org:10.4049/jimmunol.1302783
32. Turner, J. S. *et al.* SARS-CoV-2 mRNA vaccines induce persistent human germinal centre responses. Nature **596**, 109–113 (2021). https://doi.org:10.1038/s41586-021-03738-2
33. Greinacher, A. *et al.* Insights in ChAdOx1 nCoV-19 vaccine-induced immune thrombotic thrombocytopenia. Blood **138**, 2256–2268 (2021). https://doi.org:10.1182/blood.2021013231
34. Butler, A., Hoffman, P., Smibert, P., Papalexi, E. & Satija, R. Integrating single-cell transcriptomic data across different conditions, technologies, and species. Nat Biotechnol **36**, 411–420 (2018). https://doi.org:10.1038/nbt.4096
35. Frolich, D. *et al.* Secondary immunization generates clonally related antigen-specific plasma cells and memory B cells. J Immunol **185**, 3103–3110 (2010). https://doi.org:10.4049/jimmunol.1000911
36. Rincon-Arevalo, H. *et al.* Impaired humoral immunity to SARS-CoV-2 BNT162b2 vaccine in kidney transplant recipients and dialysis patients. Sci Immunol **6** (2021). https://doi.org:10.1126/sciimmunol.abj1031
37. Hein, S. *et al.* Quantitative and Qualitative Difference in Antibody Response against Omicron and Ancestral SARS-CoV-2 after Third and Fourth Vaccination. Vaccines (Basel) 10 (2022). https://doi.org:10.3390/vaccines10050796

Figures

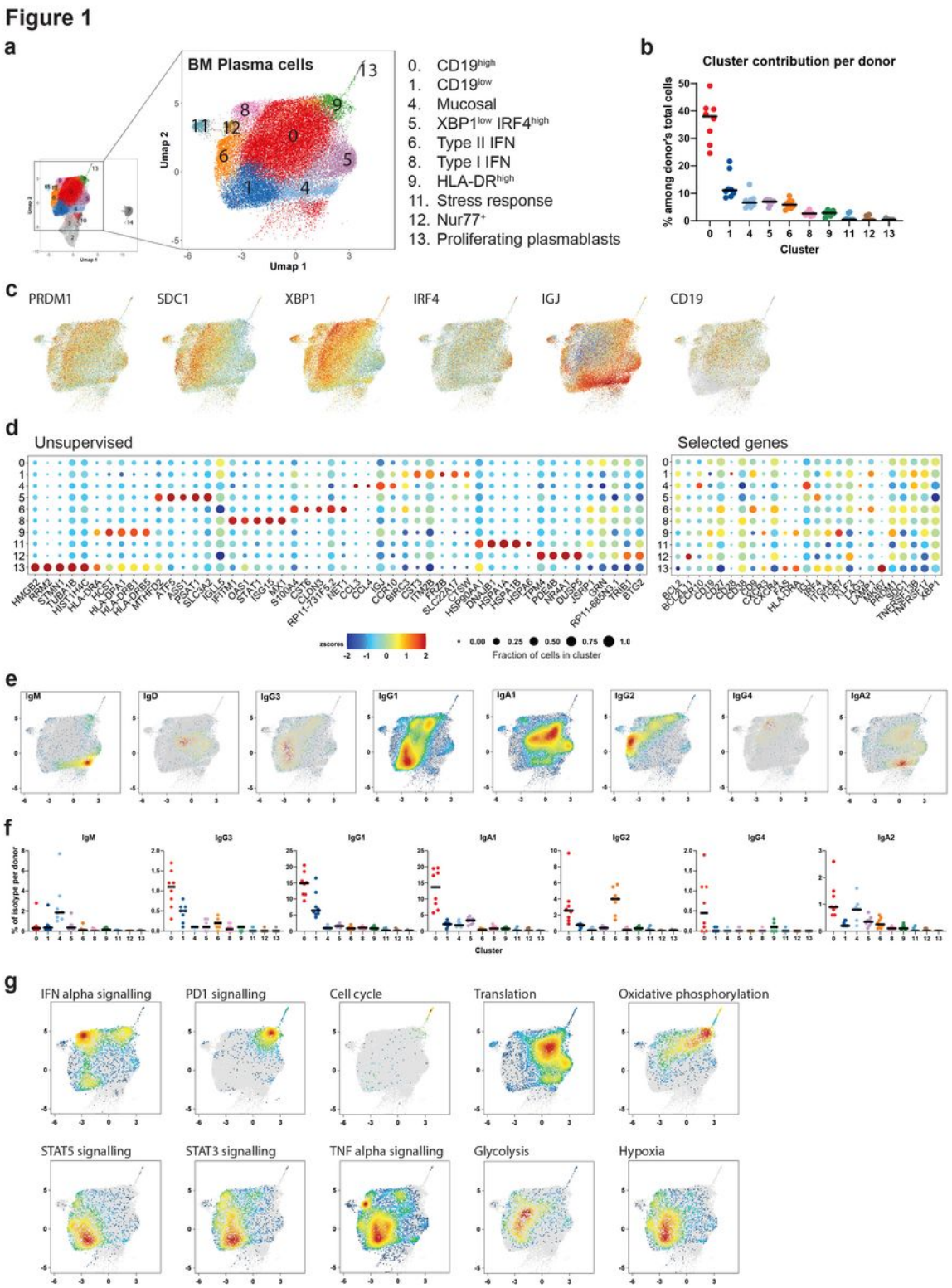

Figure 1

Transcriptional and functional heterogeneity of BMPC

a) Bone marrow plasma cells (BMPC; CD138^{high} CD38^{high} or CD38^{high} CD27^{high}) from 8 patients undergoing total hip replacement were isolated and sorted by FACS for single cell sequencing (gating strategy in Supplementary Figure 1a). Amplified area: UMAP representation of 38235 sorted plasma cells

after exclusion of contaminant and poor quality cells (see Supplementary Figure 1b). Transcriptionally similar clusters were identified using shared nearest neighbour (SNN) modularity optimization.

b) Percentage of BMPC found in each cluster per donor's total cells analysed. Horizontal lines indicate the median.

c) UMAP representation of the expression levels of selected PC signature genes across BMPC subsets.

d) Left: Bubble plot of the expression of the top ten marker genes as found by differential expression analysis (unsupervised). Right: Bubble plot of the expression of selected genes. Colour scale shows the z-scores of the average expression of a gene within the indicated cluster. Bubble sizes correspond to the fraction of cells expressing a defined gene within the indicated cluster.

e) Density plots of immunoglobulin isotype expression within the BMPC compartment.

f) Relative distribution (frequency) of plasma cells expressing a defined immunoglobulin isotype, (displayed according to the clusters in Figure 1a, per donor's total cells where a full BCR could be identified. For better readability, each isotype was plotted separately even though the percentages are related to the total BCRs from each donor. Horizontal lines indicate the median.

g) Density plots of cells enriched for selected gene signatures based on Gene Set Enrichment Analysis (GSEA).

Figure 2

a

Cluster	Diversity	Simpson
0	9655	1
1	3786	1
4	2251	0,999
5	1852	0,999
6	1656	0,999
8	953	0,999
9	827	0,999
11	387	0,997
12	289	0,996
13	113	0,99

b

	0	1	4	5	6	8	9	11	12	13
0		9.15	6.02	5.73	4.16	3.68	2.50	1.51	1.13	0.36
1	23.32		7.42	5.84	5.36	3.25	1.98	1.14	1.08	0.32
4	25.81	12.48		7.42	9.11	3.42	3.38	1.16	1.33	0.18
5	29.86	11.93	9.02		6.32	4.21	2.97	2.27	1.40	0.49
6	24.28	12.26	12.38	7.07		4.35	4.17	1.39	1.45	0.48
8	37.25	12.91	8.08	8.18	7.56		3.88	2.94	2.20	0.52
9	29.14	9.07	9.19	6.65	8.34	4.47		1.45	1.69	1.33
11	37.73	11.11	6.72	10.85	5.94	7.24	3.10		1.29	0.52
12	37.72	14.19	10.38	9.00	8.30	7.27	4.84	1.73		0.35
13	30.97	10.62	3.54	7.96	7.08	4.42	9.73	1.77	0.88	

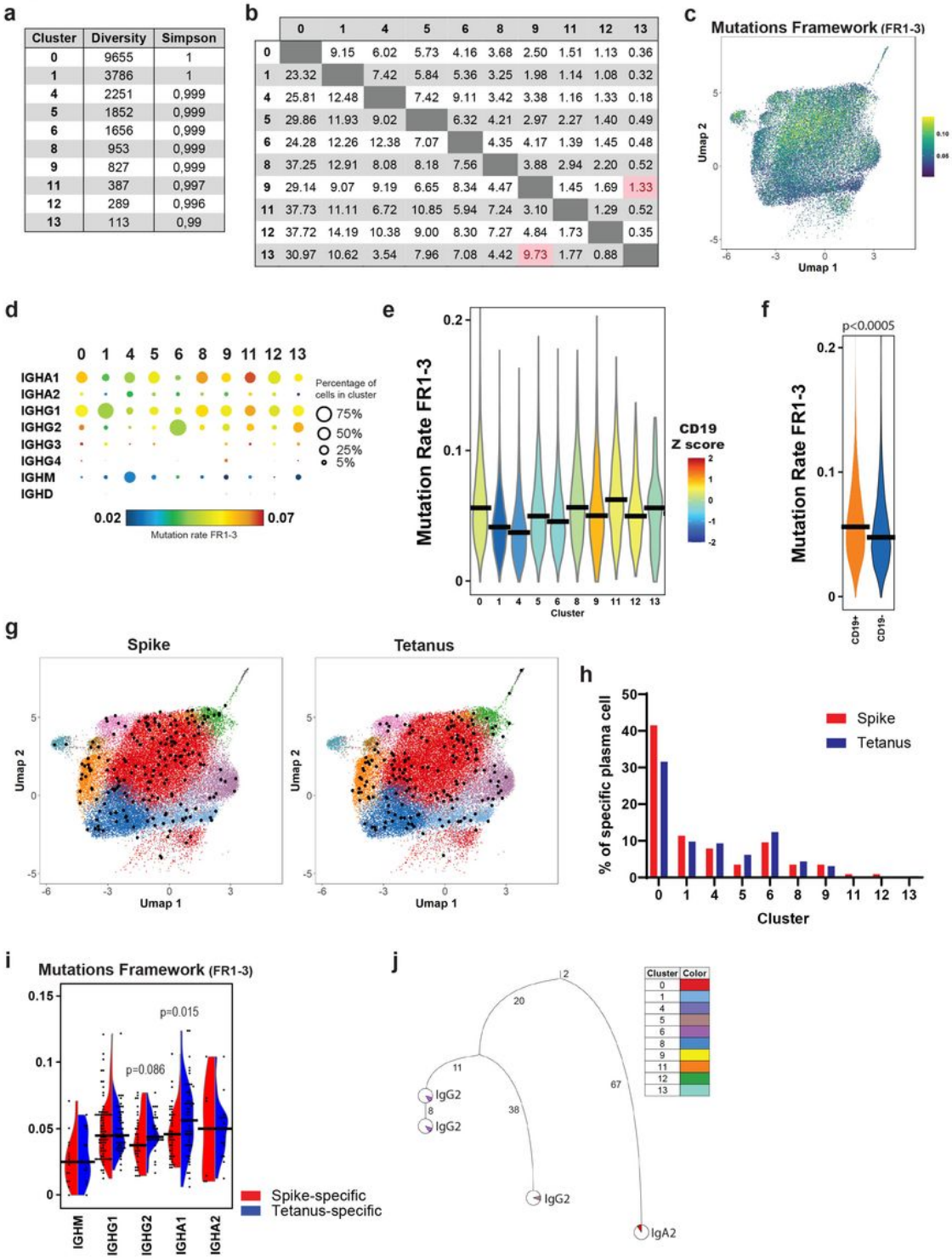

Figure 2

BMPC are clonally diverse and present different mutation rates between CD19^{high} and CD19^{low} compartments

a) Number of clonal families of BCRs found in the different clusters of analysed BMPC (diversity) and probability of finding different clonal families by random selection (Simpson diversity index). A clonal

family was defined by same germline sequence of the FR1-CDR1-FR2-CDR2-FR3 region, V and J gene as well as the length of the CDR3 region in both the heavy and light chains.

b) Overlap between clusters based on clonally related sequences. Numbers correspond row-wise to the percentage of clonal families in the particular cluster co-occurring in a different cluster (column). Red values indicate statistically significant higher overlaps than expected by 1000 randomizations. p-values shown in Supplementary data. Frequencies of clonal families were not considered.

c) Mutation rates in the framework regions FR1-3 of the heavy and light chains of the V(D)J rearrangements across BMPC clusters.

d) Bubble plot of the mutation rates in the framework regions FR1-3 of BCRs per isotype and cluster. Colour scale indicates median mutation rates. Bubble sizes correspond to the percentage of cells expressing a defined isotype within the indicated cluster.

e) Violin plot depicting the mutation rates in framework regions FR1-3 of BMPC per cluster. No significant differences between clusters were found. Horizontal lines represent the median mutation rate. Violins are coloured by the z-score of CD19 gene expression in each cluster.

f) Comparison of mutation rates in the framework regions FR1-3 of $CD19^+$ and $CD19^-$ BMPC from all clusters. Horizontal lines represent the median mutation rate. P value from Mann-Whitney-U Test.

g) Identification of SARS-CoV-2 spike-specific and tetanus toxoid-specific public clones (in black) among analysed BMPC. Public clones were defined by comparison of clonal families as found in BCR sequencing of sorted peripheral blood and bone marrow spike- and tetanus-specific cells from vaccinated individuals (see Supplementary Figure 1a and Supplementary Table 2).

h) Relative distribution of spike-specific (red) and tetanus-specific (blue) BMPC (depicted in Figure 2g) per cluster.

i) Comparison of mutation rates within the framework regions FR1-3 of spike-specific (red) and tetanus-specific (blue) BMPC per isotype. Horizontal lines represent the median mutation rate. P value from Mann-Whitney-U Test.

j) Clonal relatives of a selected SARS-CoV-2 spike-specific clonal family from public clones identified in BMPC. A clonal family comprises clones with the same germline FR1-CDR1-FR2-CDR2-FR3 sequence, used V-, J- genes and the length of the cdr3 region in both heavy and light chain. Mutation tree is based on the FR1-CDR1-FR2-CDR2-FR2 sequence. Each pie chart represents at least one clone with a particular sequence. Numbers indicate the nucleotide mutation distance to their next common ancestor. Colour in the pie chart indicates in which BMPC cluster the clone was identified. Clone isotypes are indicated next to the respective pie chart.

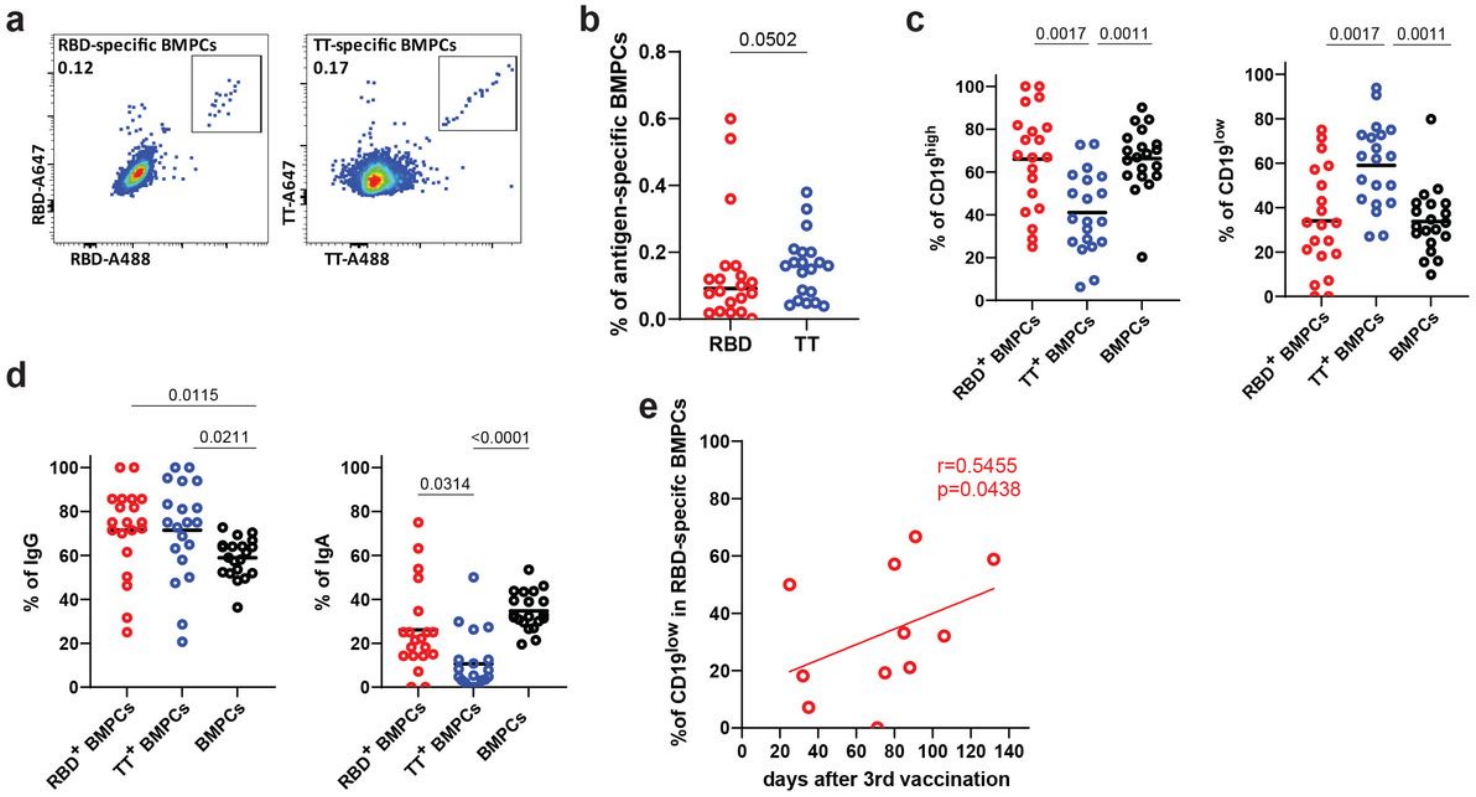

Figure 3

RBD and tetanus-specific BMPC localize preferentially in distinct CD19 compartments

a) Representative pseudocolour plots of intracellular SARS-CoV-2 RBD or tetanus toxoid (TT) staining in $CD38^{high}CD138^{+}CD14^{-}CD3^{-}$ live singlet BMPC (gating strategy in Supplementary Figure 3a), showing double-positive RBD-specific BMPC (left) and TT-specific BMPC (right).

b) Frequencies of RBD-specific and TT-specific BMPC (gates shown in Figure 3a) within total BMPC. Horizontal lines indicate the median. P value from one-tailed Mann Whitney U test. Each symbol represents one donor/sample (n=20).

c) Frequencies of $CD19^{high}$ (left) and $CD19^{low}$ (right) cells within RBD-specific BMPC (red), TT-specific BMPC (blue) and total BMPC (black). Horizontal lines indicate the median. P values from Kruskal-Wallis tests with Dunn's correction for multiple comparisons. Each symbol represents one donor/sample (n=20).

d) Frequencies of IgG+ (left) and IgA+ (right) cells within RBD-specific BMPC (red), TT-specific BMPC (blue) and total BMPC (black). Horizontal lines indicate the median. P values from Kruskal-Wallis tests with Dunn's correction for multiple comparisons. Each symbol represents one donor/sample (n=20).

e) Correlation between the frequency of $CD19^{low}$ RBD-specific BMPC and days after 3rd vaccination against SARS-CoV-2. P and r values from one-tailed Spearman's correlations. Each symbol represents one

donor/sample (n = 11).

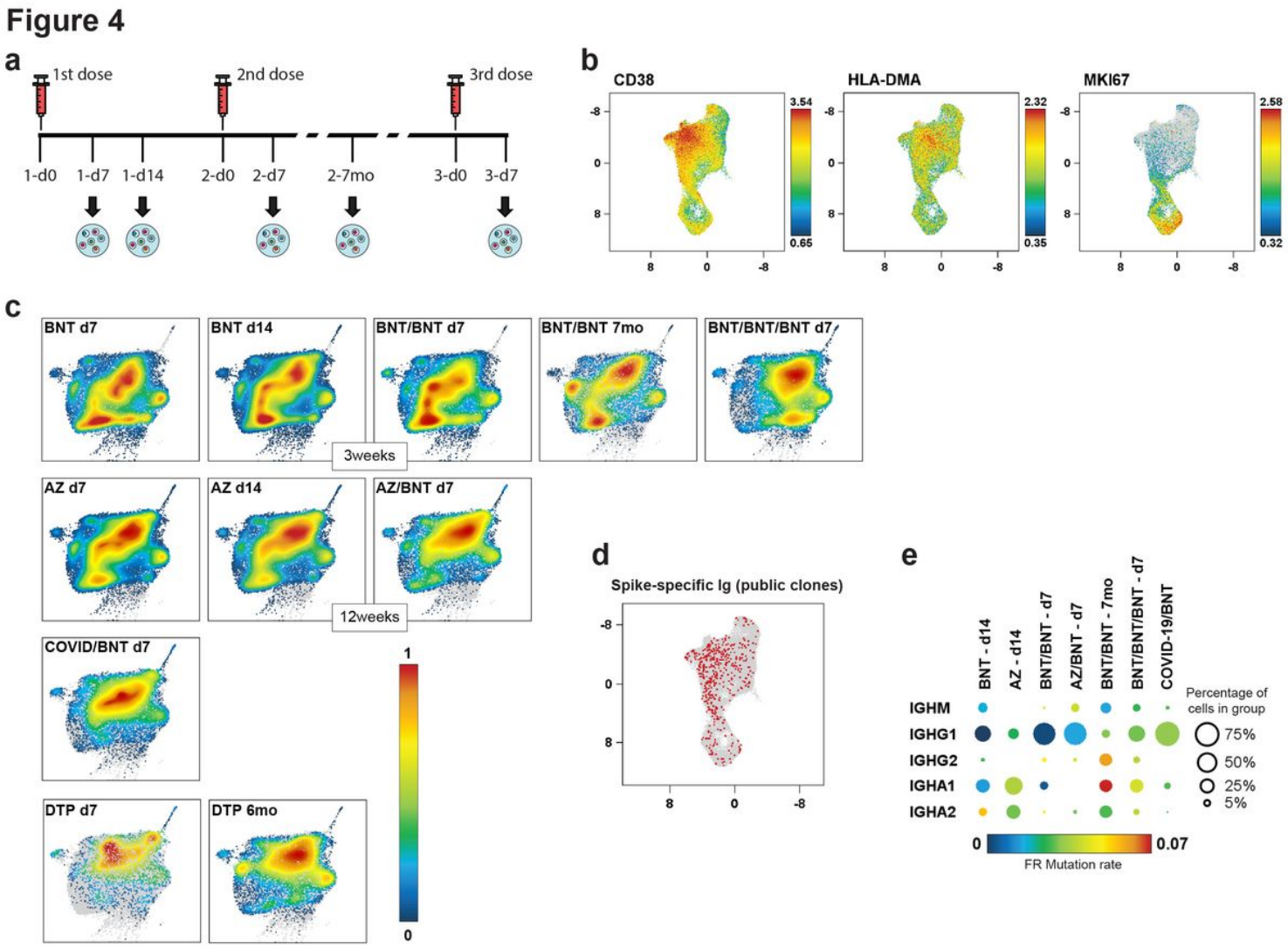

Figure 4

Type and timing of B cell activation imprints on BMPC subsets

a) Schematic representation of vaccination, blood collection and single cell sequencing time points. Arrows indicate time points of transcriptome and full-length B cell receptor (BCR) repertoire sequencing.

b) UMAP representation of the expression levels of selected genes in 55071 CD27^{high}CD38^{high} sorted peripheral blood ASC from 35 healthy individuals after COVID-19 or diphtheria, tetanus, pertussis (DTP) vaccination (see Supplementary Table 3 for information on subjects and different vaccination schemes). Colour scale represents the expression level of the indicated genes.

c) Density plots of BMPC with significant enrichment in a Gene Set Enrichment Analysis (GSEA) of gene signatures from peripheral blood ASC isolated at different time points after vaccination (as shown in Figure 4a).

d) Identification of SARS-CoV-2 spike-specific (red) public clones among analysed ASC. Public clones were defined by sharing same clonal family as experimentally verified specific clones. Clonal family was defined by the same germline sequence between FR1-FR3 region, VJ gene and length of the CDR3 region in both heavy and light chain of the BCR gene rearrangements. Specific cells were identified by BCR sequencing of sorted peripheral blood and bone marrow spike-specific cells from vaccinated individuals (see Supplementary Figure 1a and Supplementary Table 2).

e) Bubble plot of mutation rates in framework regions FR1-3 of identified spike-specific public clones (Figure 4d) per isotype identified in time point after COVID-19 vaccination. Colour scale indicates median mutation rates. Bubble sizes correspond to the percentage of cells expressing a defined isotype within the indicated group.

Supplementary Files

This is a list of supplementary files associated with this preprint. Click to download.

- SupplementaryTable1.xlsx
- SupplementaryTable2.xlsx
- SupplementaryTable3.xlsx
- SupplementaryTable4.xlsx
- SupplementaryTable5.xlsx
- SupplementaryDatastatistics.xlsx
- SupFigure1.pdf
- SupFigure2.pdf
- SupFigure3.pdf
- SupFigure4.pdf